Aerosol Science and Technology

ISSN: 0278-6826 (Print) 1521-7388 (Online) Journal homepage: informahealthcare.com/journals/uast20

Seasonal Variation of Airborne Particle Deposition Efficiency in the Human Respiratory System

Walter A. Ham, Chris R. Ruehl & Michael J. Kleeman

To cite this article: Walter A. Ham, Chris R. Ruehl & Michael J. Kleeman (2011) Seasonal Variation of Airborne Particle Deposition Efficiency in the Human Respiratory System, Aerosol Science and Technology, 45:7, 795-804, DOI: 10.1080/02786826.2011.564239

To link to this article: https://doi.org/10.1080/02786826.2011.564239

Aerosol Science and Technology, 45:795–804, 2011

ISSN: 0278-6826 print / 1521-7388 online
DOI: 10.1080/02786826.2011.564239

Seasonal Variation of Airborne Particle Deposition Efficiency in the Human Respiratory System

Walter A. Ham, Chris R. Ruehl, and Michael J. Kleeman
Department of Civil and Environment Engineering, University of California, Davis, California, USA

Particulate matter (PM) is associated with human health effects but the apparent toxicity of PM in epidemiological studies varies with season. PM toxicity may change due to seasonal shifts in composition or particle size distributions that in turn affect respiratory deposition efficiencies. In the current study, size-resolved PM composition was measured in the largest city (Fresno) in California's heavily polluted San Joaquin Valley during the summer (30 days) and winter (20 days) between 2006 and 2009 for 21 metals, organic carbon, elemental carbon, and 7 water-soluble ions. The Multiple-Path Particle Dosimetry model was applied to determine if seasonal variation in size-resolved composition influences respiratory deposition patterns. Mg, Al, S, V, Mn, Fe, Ni, Ba, SO_4^{2-}, Na^+, and Ca^{2+} had larger total deposition efficiencies ($p < 0.004$) during the summer versus the winter in all three regions of the respiratory tract. This trend results from increased relative concentrations of the target analytes per $\mu g\ m^{-3}$ ambient $PM_{1.8}$ concentration and would be detected with routine $PM_{2.5}$ filter samples. V, Zn, Se, NO_3^-, SO_4^{2-}, and NH_4^+ also experienced seasonal size distribution shifts that enhanced the specific deposition efficiency in the tracheobronchial and pulmonary regions during the summer months ($p < 0.05$). This enhanced deposition would not be detected by routine filter samples because all of the size distribution changes occur at particle diameters <2.5 μm. This study demonstrates that changes to the particle size distributions (<2.5 μm) can enhance respiratory deposition efficiencies for trace metals and/or water-soluble ions and this may contribute to seasonal shifts in PM toxicity.

Received 30 July 2010; accepted 21 January 2011.

This research was funded by the United States Environmental Protection Agency under contract R832414-010 to the University of California, Davis. Although the research described in the article has been funded by the United States Environmental Protection Agency, it has not been subject to the agency's required peer and policy review and therefore does not necessarily reflect the reviews of the agency and no official endorsement should be inferred. Further support for this research was provided by the University of California Toxic Substances Research and Teaching Program (TSR&TP) through the Atmospheric Aerosols and Health Lead Campus Program (aah.ucdavis.edu) and the Gates Millennium Scholars Program.

Address correspondence to Michael J. Kleeman, Department of Civil and Environmental Engineering, University of California, One Shields Avenue, Davis, California 95616, USA. E-mail: mjkleeman@ucdavis.edu

[Supplementary materials are available for this article. Go to the publisher's online edition of *Aerosol Science and Technology* to view the free supplementary files.]

INTRODUCTION

Recent epidemiological studies have demonstrated correlations between increased concentrations of airborne particulate matter (PM) with aerodynamic diameter (D_p) less than 2.5 μm ($PM_{2.5}$) and adverse health effects (Laden et al. 2000; Pope and Dockery 2006). $PM_{2.5}$ is a complex environmental contaminant characterized by a diverse array of chemical and physical properties that can be broadly described by particle composition, size, and shape. There does not appear to be a consensus on which PM characteristics are the most important for acute and chronic health effects but numerous research studies are underway to address this question (Health Effects Institute (HEI) 2002). In one such study, Franklin et al. (2008) used data from the EPA Technology Transfer Network Air Quality System and daily mortality records from the National Center for Health Statistics to demonstrate that $PM_{2.5}$ toxicity varies significantly by season and location across the United States. They went on to determine that increased proportions of PM aluminum (Al), nickel (Ni), arsenic (As), silicon (Si), and sulfate (SO_4^{2-}) enhanced the mass mortality association while nitrate (NO_3^-) reduced the effect. This suggests that seasonal changes in the chemical composition of $PM_{2.5}$ may provide a signal that can be used to identify the properties of airborne particles that determine their overall toxicity.

A second factor that may contribute to the observed seasonal variation in PM toxicity is seasonal changes to PM size distribution leading to altered deposition efficiencies in the respiratory system. This effect has not been explored to date; previous studies have examined the relationship between PM size *or* composition with health effects data, but few studies have simultaneously correlated PM size *and* chemical composition with health effects (HEI 2002). Idealized size distribution data and laboratory-generated aerosol size distribution data have been used to calculate respiratory deposition efficiencies (Nazaroff et al. 1993; Venkataraman and Raymond 1998; Alfoldy et al. 2009) but very few studies have utilized ambient-size-resolved

composition data obtained through field experiments (Szoke et al. 2007) due to the time and cost required to collect these measurements.

In the current study, seasonal changes to the respiratory deposition patterns of outdoor airborne PM induced by changes to particle size and composition are calculated at Fresno, CA. Fresno is the largest city in California's San Joaquin Valley (SJV), which is one of the most heavily polluted air basins in the United States. Measurements of PM composition in size fractions ranging from $PM_{0.1}$ to $PM_{1.8}$ made over twelve experiments between 2006 and 2009 are combined with a human airway deposition model (Multiple-Path Particle Dosimetry (MPPD) model, MPPD v 2.0; Asgharian and Anjilvel 1998) to estimate deposition patterns within each region of the respiratory system. Results are reported for twenty-one trace species (Na, Mg, Al, P, S, K, Ca, Ti, V, Mn, Fe, Ni, Cu, Zn, As, Se, Br, Sn, Sb, Ba, and Pb), organic carbon (OC), elemental carbon (EC), and major water-soluble ions (Cl^-, NO_3^{2-}, SO_4^{2-}, Na^+, NH_4^+, K^+, and Ca^{2+}). Deposition mass for each species is compared to total $PM_{1.8}$ concentrations (since fine PM is typically used during epidemiological studies) to detect seasonal patterns. The effect of seasonal changes to particle size distributions versus seasonal changes to particle composition are compared as possible explanations for the apparent increase in toxicity of summertime PM at Fresno.

METHODS

Airborne PM samples were collected at the boundary between a commercial development (100 m south) and residential neighborhoods (10 m north) adjacent to a busy regional highway, CA-41 (400 m west) in Fresno, CA. Eight PM samples were collected over 30 summer days (July–August) and 4 PM samples were collected over 20 winter days (January–February) between 2006 and 2009. Sample collection occurred between 9 am and 3 pm on each sample day (Sunday–Thursday) alongside health exposure studies. The results of these exposure studies have been reported elsewhere (den Hartigh et al. 2010; Ngo et al. 2010; Wilson et al. 2010).

PM samples were collected using six Micro-Orifice Uniform Deposit Impactors (MOUDI model 110, MSP Corp.) and three Reference Ambient Air Samplers (RAAS2.5-400, Andersen). Air and Industrial Hygiene Laboratory (AIHL) cyclone separators (John and Reischl 1980) were operated upstream of all samplers to remove particles with $D_p > 1.8\ \mu$m, which are prone to bounce artifacts. Three MOUDIs were operated with Teflon (R2PJ047, Pall Corp.) substrates and after filters for parallel gravimetric, water-soluble ions, and trace metals analysis. The remaining three MOUDIs were operated with aluminum foil substrate and quartz fiber after filters for gravimetric (foil) and carbonaceous (foil and quartz) analysis. RAAS measurements were used to provide quality control and quality assurance of all integrated MOUDI measurements.

PM mass concentrations were measured by preweighing and postweighing Teflon and foil substrates with a CAHN-33 microbalance in a temperature and relative humidity controlled room. OC and EC were measured on quartz filters and aluminum substrates with the NIOSH 5040 thermo-optical method using a Sunset Laboratory OC/EC analyzer. One half of each Teflon filter was extracted for ion chromatography (IC) analysis, and the other half was extracted for inductively coupled plasma mass spectrometer (ICP-MS) analysis. Filter halves designated for IC were extracted with a 1% Ultima-grade ethanol solution made with ultrapure water (MilliQ) and analyzed with a Dionex DX-600 IC system to measure Cl^-, NO_3^-, SO_4^{2-}, Na^+, NH_4^+, K^+, and Ca^{2+}. Filter halves designated for ICP-MS were extracted with a mixture of 75% acetone (Fisher Optima grade) and 25% 1 N nitric acid (Fisher trace metal grade diluted with MilliQ ultrapure water) and analyzed for trace elements (Na, Mg, Al, P, S, K, Ca, Ti, V, Mn, Fe, Ni, Cu, Zn, As, Se, Br, Sn, Sb, Ba, and Pb) with ICP-MS (Agilent 7500i). Further details of the chemical analysis procedures are provided by Herner, Green, et al. (2006). Mass median aerodynamic diameter (MMAD) and geometric standard deviation (GSD) values for each species were calculated from MOUDI filter measurements using a log-probit method described by O'Shaughnessy and Raabe (2003).

Airway deposition calculations were carried out using the MPPD model. MPPD is a commercially available computational dosimetry model developed by the Chemical Industry Institute of Toxicology (CIIT) and the Dutch National Institute of Public Health and the Environment (RIVM) that can be used for estimating human and rat airway particle dosimetry. This model can calculate the deposition efficiencies for PM deposition and clearance by diffusion, sedimentation, and impaction within airway bifurcations. The MPPD model has been successfully used in previous studies to estimate particle dosimetry and is ideally suited for estimating deposition using size-resolved chemical speciation data (Oberdorster et al. 2004; Elder and Oberdorster 2006; Nong et al. 2009). Model adjustable assumptions used in this work include spherical particles, nose-only breathing, a tidal volume of 625 mL, and a breathing frequency of 12 breaths/min to simulate the respiratory system of an average human adult. These parameters are considered typical for the general population but they may not accurately represent susceptible populations such as children and those with compromised respiratory systems. The amount of deposited $PM_{1.8}$ mass of each species was estimated as follows:

1. Used MPPD to calculate size-resolved deposition fractions for each region of the respiratory tract.
2. Calculated the areas under the deposition fraction curves separated for each MOUDI size bin to yield a MOUDI-size-resolved deposition fraction.
3. Multiplied the mass of a species measured in a MOUDI size bin by the corresponding MOUDI-size-resolved deposition fraction to find the deposited mass of a species in each MOUDI size bin.

TABLE 1
Average concentration, MMAD, and GSD of measured species during the Fresno summer and winter sampling events. Note that trace element concentrations are shown in ng m^{-3} while OC, EC, and water-soluble ions are shown in μg m^{-3}

	Fresno summer				Fresno winter			
	Average concentration	Standard deviation	MMAD (μm)	GSD (μm)	Average concentration	Standard deviation	MMAD (μm)	GSD (μm)
Trace species (ng m^{-3})								
Na	76.7	54.6	0.84	6.34	57.2	58.9	0.59	3.29
Mg	12.3	7.96	1.52	2.49	3.49	2.41	0.80	3.12
Al	48.2	70.3	0.31	2.00	34.7	31.1	0.73	3.82
P	10.7	12.7	0.42	2.09	63.5	76.6	0.45	3.52
S	782	592	0.35	2.08	512	361	0.54	2.46
K	8.02	7.02	0.65	1.75	18.2	8.77	0.45	2.24
Ca	9.01	12.1	0.70	8.57	8.22	3.39	0.47	3.91
Ti	1.26	0.69	1.27	2.61	2.51	2.32	1.43	3.10
V	0.12	0.07	0.47	1.58	0.04	0.03	0.56	2.54
Mn	1.01	0.65	0.94	2.39	0.91	0.71	0.69	1.23
Fe	30.8	28.3	1.18	3.27	29.1	22.1	1.99	3.70
Ni	11.7	18.8	2.71	3.01	4.92	3.19	0.33	4.85
Cu	1.00	1.04	0.80	3.62	1.85	0.97	1.16	4.09
Zn	8.97	8.27	0.55	4.23	31.6	36.3	0.46	2.57
As	0.13	0.12	0.34	1.71	0.25	0.14	0.34	1.84
Se	0.19	0.19	0.85	1.80	0.10	0.01	0.54	1.19
Br	4.72	2.42	0.31	1.80	7.31	6.29	0.45	1.81
Sn	1.16	1.31	0.30	1.67	3.20	2.90	0.51	2.70
Sb	0.56	0.57	0.53	2.21	2.43	1.72	0.67	2.13
Ba	2.59	2.25	1.02	2.54	1.53	0.93	1.55	2.88
Pb	0.25	0.15	0.32	1.56	0.76	0.28	0.34	2.59
Major species (μg m^{-3})								
OC	3.86	1.95	0.31	1.70	4.66	0.97	0.30	1.97
EC	0.54	0.29	0.23	1.80	0.79	0.40	0.26	1.71
Cl^-	0.08	0.08	0.50	2.16	0.05	0.01	0.45	2.85
NO_3	0.75	0.64	0.58	2.21	10.8	7.81	0.54	1.60
SO_4	1.66	0.60	0.33	1.58	1.19	0.50	0.50	1.82
Na^+	0.11	0.08	0.76	2.93	0.06	0.03	0.64	3.06
NH_4^+	0.68	0.25	0.33	1.78	3.19	2.01	0.51	1.56
K^+	0.03	0.05	0.46	2.46	0.05	0.04	0.40	1.59
Ca_2^+	0.02	0.01	0.42	2.02	0.01	0.01	0.59	2.33

4. Summed the deposited masses found in each MOUDI size bin to yield an integrated $PM_{1.8}$ deposition total.

Figure S1 (supplemental information) shows MPPD model predictions for the deposition fraction of polydisperse aerosol in a typical human respiratory tract. Deposition curves are shown for the head airways, the tracheobronchial region, and the pulmonary region for particles with MMAD ranging from 1 nm to 10 μm. Vertical lines indicate stage cut-sizes for the MOUDIs used in this experiment. Relatively large particles ($D_p > 0.56$ μm) deposit in the head airways ($\sim$22%) as a result of sedimentation and the impaction of particles onto the larynx and airway bifurcations (Lee and Wang 1975; Wang 1975; Cai and Yu 1988; Zhang and Yu 1993). Deposition of particles with $D_p < 0.18$ μm is primarily governed by Brownian diffusion (Ingham 1984) leading to preferential deposition in the pulmonary region ($\sim$21%) followed by the head airways ($\sim$18%) and then the tracheobronchial region ($\sim$13%).

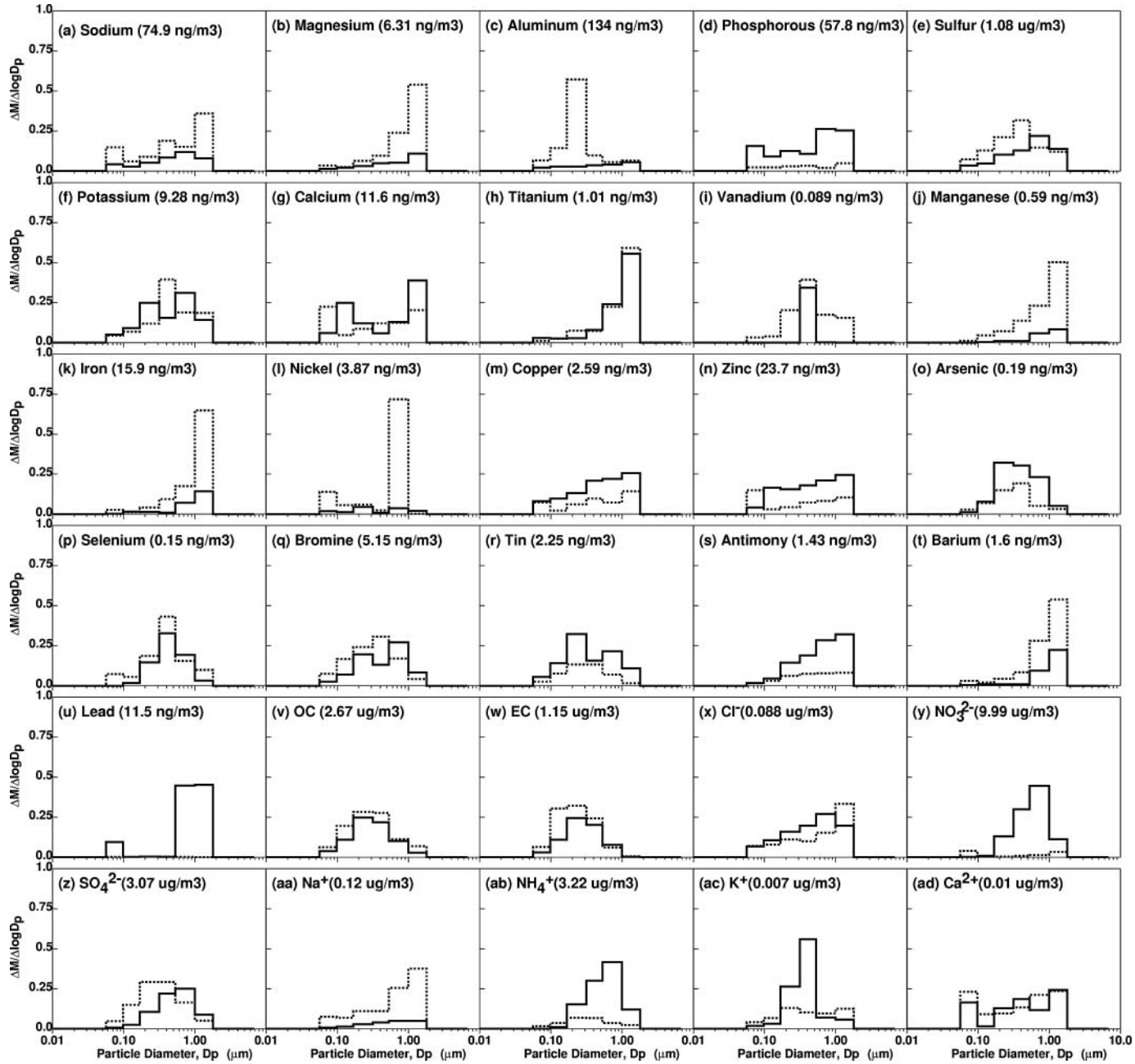

FIG. 1. Relative MOUDI size distributions of individual species. Concentrations are normalized to maximum observed $PM_{1.8}$ concentrations (values in the parenthesis). Dashed lines represent summer while solid lines represent winter.

Particles with 0.18 μm $< D_p <$ 0.56 μm are not easily deposited in the respiratory system resulting in small deposition fractions ($\sim$10%).

Respiratory deposition efficiency was the primary metric calculated in the current study because fine particle species concentrations and total mass are typically the independent variables employed in epidemiological analyses (Dominici et al. 2005; Franklin et al. 2007; Ostro et al. 2007). Respiratory deposition was regressed against $PM_{1.8}$ total mass concentrations yielding a "total deposition efficiency" (with units of ng of each species deposited per μg ambient $PM_{1.8}$ total mass). Respiratory deposition was also regressed against individual $PM_{1.8}$ species concentrations yielding a "specific deposition efficiency" (with units of ng of each species deposited per ng ambient $PM_{1.8}$ species mass). The total deposition efficiency changes in response to both species size distributions and species relative concentrations while the specific deposition efficiency only changes in response to species size distributions. Respiratory deposition

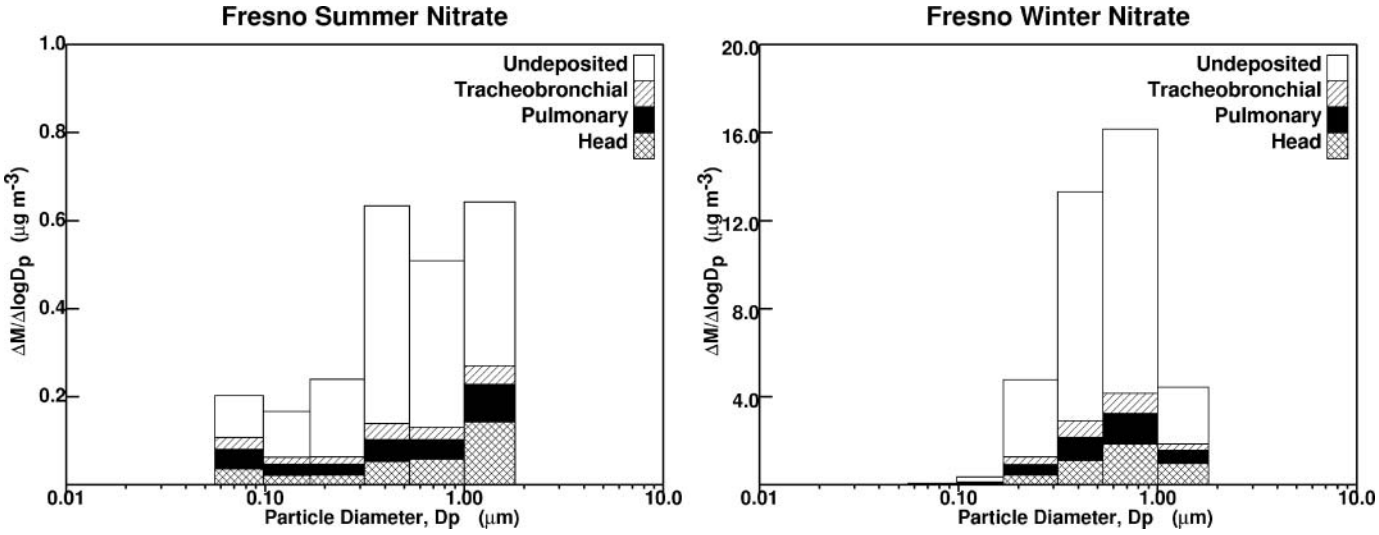

FIG. 2. Average MOUDI nitrate size distribution and respiratory deposition fractions during the Fresno summer and winter sampling events.

efficiencies were calculated separately for summer and winter events for all measured species to quantify seasonal differences. A student's *t*-test with the Bonferroni correction was performed to calculate p values for all measured species. These p values show whether or not deposition efficiencies for each species are significantly different between the summer and winter months at the 95% confidence interval (CI).

RESULTS

Table 1 contains average integrated $PM_{1.8}$ mass concentrations, MMAD, and GSD values for all species measured. Average $PM_{1.8}$ total mass concentrations for the summer and winter events were 16.6 and 23.1 μg m^{-3}, respectively. OC was the dominant PM species during the summer months with an average mass concentration of 3.86 μg m^{-3}, while NO_3^- was the major species during the winter events with a mass concentration of 10.8 μg m^{-3}. NH_4^+ was more prevalent in the winter than in the summer (3.19 μg m^{-3} vs. 0.68 μg m^{-3}), which was expected because of the seasonal variation in NO_3^- observed in the SJV. Elements more abundant in the summer included Na, Mg, Al, Ni, Se, V, and Ba, while concentrations of P, K, Ti, Zn, As, Sn, Sb, Cu, Br, and Pb were greater in the winter. The remaining species (OC, EC, Ca, Mn, and Cl) had similar concentrations in both the seasons. These PM speciation measurements agreed favorably with measurements made at the US EPA Speciation Trend Network (STN) site located in Fresno on the study days of interest (Figure S2). The sampling duration of 9 am to 3 pm used for the current study therefore appears to adequately represent daily averages for the present analysis.

Figure 1 shows average size distributions of trace metals, OC/EC, and water-soluble ions measured in the current study. These size distributions were generated by averaging three colocated MOUDIs (each with 7 size fractions) collected during 8 summer and 4 winter sampling periods. Note that size distribution plots are normalized to the values in parenthesis in each subfigure to simplify the vertical axis. Size distributions for Na, Mg, Al (winter only), Ti, Mn, Fe, Cu, Zn, and Ba appear to peak in larger size fractions ($D_p > 0.56$ μm) indicating that these PM species were formed through mechanical abrasion processes (Seinfeld and Pandis 1998). Many of these elements are present in crustal material (Warneck 1988) and their concentrations are generally greater in the summer months when soil moisture is reduced suggesting windblown dust as one possible source. Two water-soluble ions (Na^+, NO_3^-) appear to peak in larger size fractions ($D_p > 0.56$ μm) during the summer months with a larger list of water-soluble ions (Na^+, NH_4^+, SO_4^{2-}, NO_3^-, Ca^{2+}) peaking in larger particle size fractions ($D_p > 0.56$ μm) during the winter. This seasonal pattern reflects the increased condensation of ammonium nitrate (NH_4NO_3) during the winter season causing particles to grow to larger aerodynamic diameters. NH_4NO_3 preferentially condenses onto hygroscopic particles (such as those containing SO_4^{2-}; Stelson and Seinfeld 1982) but the large amount of winter nitrate formation in the SJV generally leads to condensational growth for any particle containing water-soluble material (Herner, Ying, et al. 2006).

PM species with size distributions peaking between 0.18 and 0.56 μm are of interest since significant particle growth (thus affecting respiratory deposition patterns) can occur in this size range. Species with strong summertime peaks between 0.18 and 0.56 μm include Al, S, K, V, As, Br, Sn, OC, EC, SO_4^{2-}, and NH_4^+. Species whose wintertime size distributions peak in this size range include S, K, V, As, Sn, OC, EC, K^+, and SO_4^{2-}. Particles with diameters between 0.18 and 0.56 μm are typically emitted from combustion processes or they are formed through gas-to-particle conversion processes (Seinfeld and Pandis 1998). PM species with size distributions peaking below 0.18 μm are also of interest for health effects research because particles in

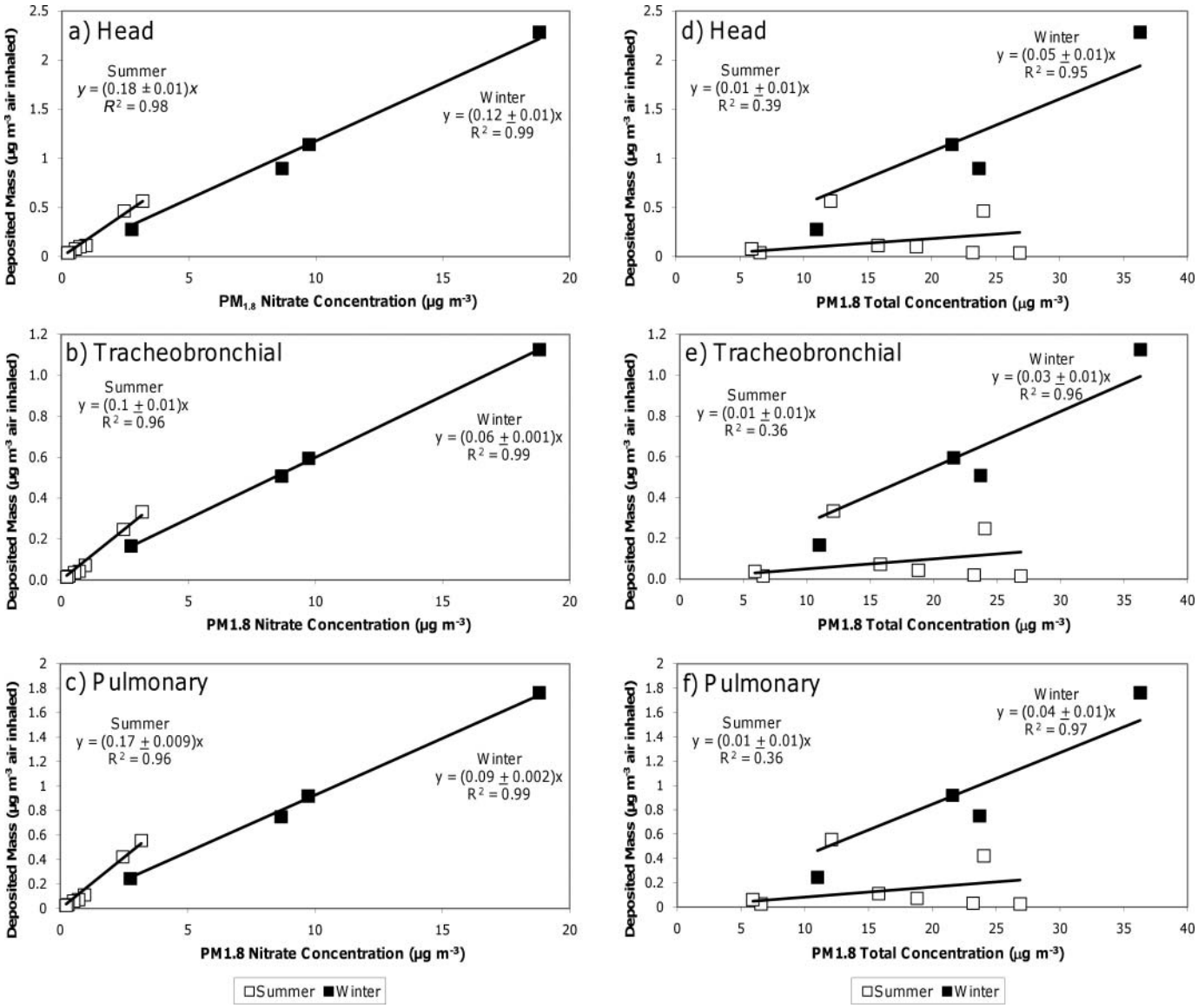

FIG. 3. (a–c) Nitrate deposition versus $PM_{1.8}$ specific nitrate concentrations and (d–f) $PM_{1.8}$ total mass concentrations during the Fresno summer and winter sampling events. Plots a, b, and c show specific deposition efficiencies while plots d, e, and f show total deposition efficiencies.

this size range may translocate through cell membranes more efficiently than larger particles (Kreyling et al. 2002; Oberdorster et al. 2002, 2004). Both Ca/Ca^{2+} and Ni size distributions have minor peaks in this size range in the summer events while Pb size distributions exhibit a minor peak during the winter months.

Figures 2 and 3 illustrate the MOUDI size distribution and respiratory deposition efficiency of nitrate during the summer and winter months. Nitrate was selected as an example for this series of calculations because nitrate experiences significantly different size distributions and concentrations between the summer and winter months in the SJV (Herner 2006b). Results for all PM components will be presented in later figures. Figure 2 illustrates that approximately 68%–75% of the nitrate present in inhaled ambient airborne particles remains undeposited for both the seasons. This undeposited material is exhaled and cleared from the respiratory tract before any deposition of PM onto respiratory surfaces occurs. Of the inhaled particulate nitrate that deposits in the respiratory system, 11%–14% remains in the head airways, 6%–7% remains in the tracheobronchial airways, and 9%–11% remains in the pulmonary regions of the lung.

Figure 3a–c show the nitrate respiratory deposition concentrations (ng nitrate deposited per m^3 air inhaled) versus ambient $PM_{1.8}$ nitrate concentrations (ng nitrate per m^3 air) during the summer (open symbols) and winter (closed symbols) sampling events. The slope of each regression line defines the specific deposition efficiency (ng nitrate deposited per ng ambient $PM_{1.8}$

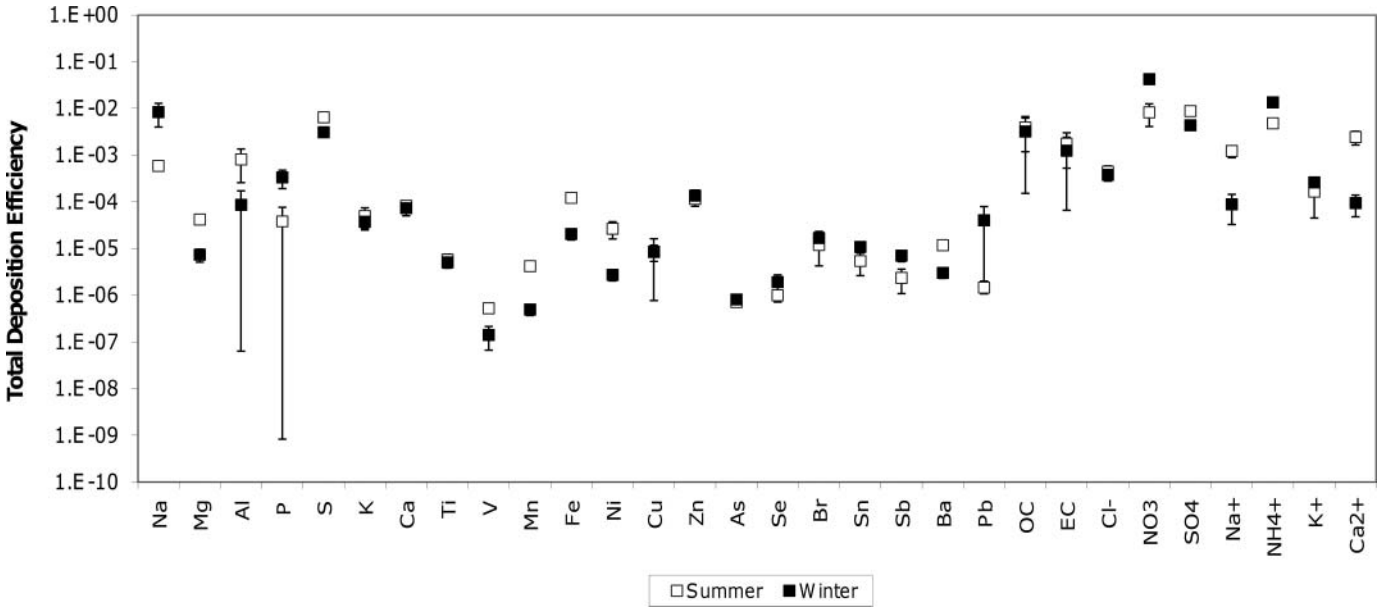

FIG. 4. Average total deposition efficiency in all regions of the respiratory tract comparing component deposition and $PM_{1.8}$ total mass concentrations using least squares method. Units are μg of each component deposited per μg $PM_{1.8}$ total mass inhaled. Error bars represent 95% CI.

nitrate inhaled). Seasonal changes to the specific deposition efficiency illustrated in subfigures (a–c) result exclusively from changes to the nitrate size distribution (see Figure 2). Nitrate respiratory deposition is highly correlated with $PM_{1.8}$ nitrate concentrations yielding a tight uncertainty range for the specific deposition efficiency. Nitrate summertime specific deposition efficiencies in the head, pulmonary, and tracheobronchial regions appear to be at least 50% greater than wintertime deposition efficiencies. The largest difference occurs in the pulmonary region where summertime deposition efficiency is nearly twice as large as wintertime efficiency (0.09 vs. 0.17). The analysis indicates that despite having similar calculated MMADs in each season, nitrate exhibits a greater specific deposition efficiency during the summer months in Fresno, CA.

Figure 3 d–f show nitrate respiratory deposition concentrations (ng nitrate deposited per m^3 air inhaled) versus ambient $PM_{1.8}$ total mass concentrations (μg total mass per m^3 air) during the summer and winter sampling events. The slope of each regression line defines the total deposition efficiency (ng nitrate deposited per μg ambient $PM_{1.8}$ total mass inhaled). Seasonal changes to the nitrate total deposition efficiency shown in Figure 3d–f can result from either a change in the ratio of nitrate to total mass or a change in the nitrate size distribution. Nitrate respiratory deposition is seasonally correlated to $PM_{1.8}$ mass concentrations because nitrate comprises a significant fraction of $PM_{1.8}$ mass in the winter but a small fraction of total $PM_{1.8}$ mass in the summer. The low summertime correlation coefficient (R^2) translates into a larger uncertainty range for the total deposition efficiency (slope) but the distinct trend of higher nitrate total deposition efficiency during the winter can still be observed with 95% CI.

Nitrate is somewhat unique because the total deposition efficiency decreases in the summer due to reduced nitrate burden in the PM but the specific deposition efficiency increases in the summer because each μg of PM nitrate that is present deposits more efficiently due to size distribution shifts. Most other PM components had total and specific deposition efficiency trends that exhibited consistent seasonal behavior. Figure 4 shows the respiratory total deposition efficiencies (μg deposited per μg $PM_{1.8}$ total mass inhaled) for all species measured in the current study using the methods illustrated in Figures 2 and 3. Error bars represent 95% CIs on the regression slope that defines the total deposition efficiency for each species. Values on the y-axis are presented using a log scale to accommodate the wide range of respiratory total deposition efficiencies. Table S1 summarizes Bonferroni-corrected p values for the specific and total deposition efficiencies calculated during these experiments. Values of p less than 0.05 show that efficiencies are significantly different between seasons at the 95% CI. Mg, Al, S, V, Mn, Fe, Ni, Ba, SO_4^{2-}, Na^+, and Ca^{2+} exhibited greater summertime versus wintertime total deposition efficiencies in the head airways, the tracheobronchial region, and the pulmonary region. The majority of this enhancement in summertime respiratory deposition was caused by an enhancement of the species concentration itself rather than from changes to size distributions. Three of these species (Al, Ni, and SO_4^{2-}) were detected as major modifiers of the $PM_{2.5}$ mass mortality association in recent epidemiological studies (Franklin et al. 2008). An additional three species with a greater respiratory total deposition efficiency in the summer (V, Mn, and Fe) were identified as minor positive modifiers of $PM_{2.5}$ toxicity. Six species (Na, P, Sb, Pb, NO_3^-, and NH_4^+) had larger respiratory total deposition efficiencies in the winter months.

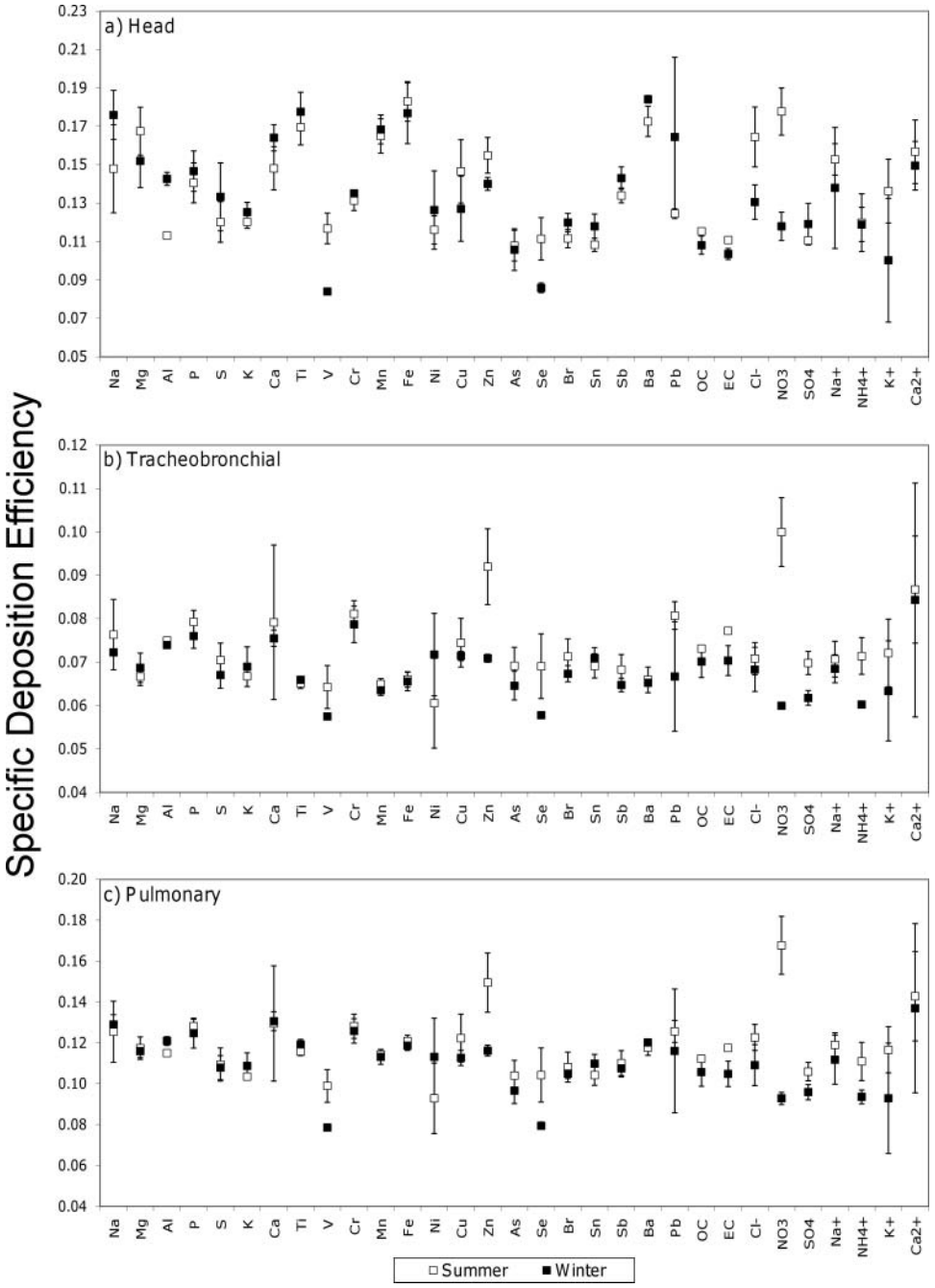

FIG. 5. Specific deposition efficiencies comparing component deposition and $PM_{1.8}$ component mass concentrations using least squares method. Units are represented as μg of each component deposited per μg $PM_{1.8}$ component mass inhaled. Error bars represent 95% CI.

Each of these species was shown to have weak or negative associations with health effects during the epidemiological analysis presented by Franklin et al. (2008).

Figure 5 shows specific deposition efficiencies (μg deposited per μg $PM_{1.8}$ species mass inhaled) in the head, tracheobronchial, and pulmonary regions of the respiratory system for all measured species during the summer and winter months. Values of p comparing the summertime and wintertime specific deposition efficiencies may be found in Table S1. Al, V, Zn, Se, Ba, Cl^-, and NO_3^- had larger specific deposition efficiencies in the head region during the summer versus winter events. Zn, Se, NO_3^-, SO_4^{2-}, and NH_4^+ had greater specific deposition efficiencies in the tracheobronchial region during the summer versus winter events. Pulmonary specific deposition efficiencies were greater in the summer than in the winter for V, Zn, Se, NO_3^-, SO_4^{2-}, and NH_4^+. Those species with greater specific deposition

efficiencies during the winter events (in the head airways only) included Al and Ba. No species had specific deposition efficiencies for the tracheobronchial region that were larger during the winter than the summer events.

DISCUSSION

Average wintertime PM concentrations in the SJV are greater than summertime concentrations but epidemiological studies indicate that summertime PM is potentially more toxic per unit of mass (Franklin et al. 2008). The findings of the current study indicate that changes to the respiratory specific deposition efficiency caused by shifts to the PM size distributions may help to explain these observed seasonal toxicity differences. Mg, Al, S, V, Mn, Fe, Ni, Ba, SO_4^{2-}, Na^+, and Ca^{2+} had larger total deposition efficiencies ($p < 0.004$) during the summer versus the winter in all regions of the respiratory tract. This trend results from increased relative concentrations of the target analytes per μg m^{-3} ambient $PM_{1.8}$ concentration and would therefore be detected with routine $PM_{2.5}$ filter samples. V, Zn, Se, NO_3^-, SO_4^{2-}, and NH_4^+ also experienced seasonal size distribution shifts that enhanced the specific deposition efficiency in the tracheobronchial and pulmonary regions during the summer months ($p < 0.05$). The seasonal size distribution shifts would not be detected by routine measurement networks that collect all PM with $D_p <$ 2.5 μm on a single filter. Epidemiological studies based solely on $PM_{2.5}$ measurements with no further size distribution information may not be sufficient for identifying the components of airborne PM responsible for adverse health effects.

It should be noted that other factors may play a role in perceived seasonal health effects such as seasonal differences in time activity and human behavior that may affect personal exposure to outdoor PM (Hanninen et al. 2005). While the current study did not account for the further seasonal modification of the ambient particle size distributions by buildings and ventilation patterns, the results may be useful to test the plausible alternative hypothesis for the seasonal shift in PM toxicity being in part due to the ambient changes in particle size distributions. The results of the current study may also provide an explanation for the apparent protective effect on human health from certain PM components such as NH_4NO_3 (Franklin et al. 2008). Protective effects are curious since plausible chemical and biological mechanisms explaining this behavior are generally lacking. If PM toxicity results solely from the chemical composition of the particles, then water-soluble salts, such as NH_4NO_3, should be nontoxic components that do not modify mortality rates. The current study suggests that PM size distribution shifts induced by the condensation of NH_4NO_3 onto primary particles reduces the deposition efficiencies of trace metals in the human respiratory system during the winter months, providing a plausible physical explanation for a protective effect. This finding has implications for nitrate control strategies in the SJV and other regions where the condensation of nitrate increases the size of primary particles. The role of condensational growth may be different in regions with lower ambient nitrate concentrations. Regions more influenced by SO_2 emissions resulting in sulfate condensation might see a similar protective effect if overall respiratory deposition rates are lowered in specific seasons.

REFERENCES

Alfoldy, B., Giechaskiel, B., Hofmann, W., and Drossinos, Y. (2009). Size-Distribution Dependent Lung Deposition of Diesel Exhaust Particles. *J. Aerosol Sci.*, 40:652–663.

Asgharian, B. and Anjilvel, S. (1998). A Multiple-Path Model of Fiber Deposition in the Rat Lung. *Toxicol. Sci.*, 44:80–86.

Cai, F. S. and Yu, C. P. (1988). Inertial and Interceptional Deposition of Spherical-Particles and Fibers in a Bifurcating Airway. *J. Aerosol Sci.*, 19:679–688.

den Hartigh, L. J., Lamé, M. W., Ham, W., Kleeman, M. J., Tablin, F., and Wilson, D. W. (2010). Endotoxin and Polycyclic Aromatic Hydrocarbons in Ambient Fine Particulate Matter from Fresno, California Initiate Human Monocyte Inflammatory Responses Mediated by Reactive Oxygen Species. *Toxicol. in Vitro*, 24:1993–2002.

Dominici, F., McDermott, A., Daniels, M., Zeger, S. L., and Samet, J. M. (2005). Revised Analyses of the National Morbidity, Mortality, and Air Pollution Study: Mortality among Residents of 90 Cities. *J. Toxicol. Environ. Health A*, 68:1071–1092.

Elder, A. and Oberdorster, G. (2006). Translocation and Effects of Ultrafine Particles outside of the Lung. *Clin. Occup. Environ. Med.*, 5:785–796.

Franklin, M., Koutrakis, P., and Schwartz, J. (2008). The Role of Particle Composition on the Association between PM2.*5 and Mortality*. *5 and Mortality*, 19:680–689.

Franklin, M., Zeka, A., and Schwartz, J. (2007). Association between PM2.5 and All-Cause and Specific-Cause Mortality in 27 US Communities. *J. Expo. Sci. Environ. Epidemiol.*, 17:279–287.

Hanninen, O. O., Palonen, J., Tuomisto, J. T., Yli-Tuomi, T., Seppanen, O., and Jantunen, M. J. (2005). Reduction Potential of Urban PM2.5 Mortality Risk Using Modern Ventilation Systems in Buildings. *Indoor Air*, 15:246–256.

Health Effects Institute (2002). *Understanding the Health Effects of Components of the Particulate Matter Mix: Progress and Next Steps*. Health Effects Institute, Cambridge, MA.

Herner, J. D., Green, P. G., and Kleeman, M. J. (2006a). Measuring the Trace Elemental Composition of Size-Resolved Airborne Particles. *Environ. Sci. Technol.*, 40:1925–1933.

Herner, J. D., Ying, Q., Aw, J., Gao, O., Chang, D. P. Y., and Kleeman, M. J. (2006b). Dominant Mechanisms that Shape the Airborne Particle Size and Composition Distribution in Central California. *Aerosol. Sci. Tech.*, 40:827–844.

Ingham, D. B. (1984). Diffusion of Aerosols from a Stream Flowing Through a Short Cylindrical Pipe. *J. Aerosol. Sci.*, 15:637–641.

John, W. and Reischl, G. (1980). A Cyclone for Size-Selective Sampling of Ambient Air. *J. Air Pollut. Control Assoc.*, 30:872–876.

Kreyling, W. G., Semmler, M., Erbe, F., Mayer, P., Takenaka, S., Schulz, H., Oberdorster, G., and Ziesenis, A. (2002). Translocation of Ultrafine Insoluble Iridium Particles from Lung Epithelium to Extrapulmonary Organs is Size Dependent but Very Low. *J. Toxicol. Environ. Health A*, 65:1513–1530.

Laden, F., Neas, L. M., Dockery, D. W., and Schwartz, J. (2000). Association of Fine Particulate Matter from Different Sources with Daily Mortality in Six US Cities. *Environ. Health Perspect.*, 108:941–947.

Lee, W. C. and Wang, C. S. (1975). Particle Deposition in Systems of Repeatedly Bifurcating Tubes. *Inhaled Part*, 4(Pt 1):49–60.

Nazaroff, W. W., Hung, W. Y., Sasse, A. G. B. M., and Gadgil, A. J. (1993). Predicting Regional Lung Deposition of Environmental Tobacco-Smoke Particles. *Aerosol Sci. Technol.*, 19:243–254.

Ngo, M. A., Pinkerton, K. E., Freeland, S., Geller, M., Ham, W., Cliff, S., Hopkins, L. E., Kleeman, M. J., Kodavanti, U. P., Meharg, E., Plummer, L., Recendez, J. J., Schenker, M. B., Sioutas, C., Smiley-Jewell, S., Haas, C.,

Gutstein, J., and Wexler, A. S. (2010). Airborne Particles in the San Joaquin Valley may Affect Human Health. *Calif. Agr.*, 64:12–16.

Nong, A., Taylor, M. D., Clewell, H. J., 3rd, Dorman, D. C., and Andersen, M. E. (2009). Manganese Tissue Dosimetry in Rats and Monkeys: Accounting for Dietary and Inhaled Mn with Physiologically Based Pharmacokinetic Modeling. *Toxicol. Sci.*, 108:22–34.

Oberdorster, G., Sharp, Z., Atudorei, V., Elder, A., Gelein, R., Kreyling, W., and Cox, C. (2004). Translocation of Inhaled Ultrafine Particles to the Brain. *Inhal. Toxicol.*, 16:437–445.

Oberdorster, G., Sharp, Z., Atudorei, V., Elder, A., Gelein, R., Lunts, A., Kreyling, W., and Cox, C. (2002). Extrapulmonary Translocation of Ultrafine Carbon Particles Following Whole-Body Inhalation Exposure of Rats. *J. Toxicol. Environ. Health A*, 65:1531–1543.

O'Shaughnessy, P. T., and Raabe, O. G. (2003). A Comparison of Cascade Impactor Data Reduction Methods. *Aerosol Sci. Technol.*, 37:187–200.

Ostro, B., Feng, W. Y., Broadwin, R., Green, S., and Lipsett, M. (2007). The Effects of Components of Fine Particulate Air Pollution on Mortality in California: Results from CALFINE. *Environ. Health Perspect.*, 115:13–19.

Pope, C. A. and Dockery, D. W. (2006). Health Effects of Fine Particulate Air Pollution: Lines that Connect. *J. Air Waste Manage. Assoc.*, 56:709–742.

Seinfeld, J. H. P. and Pandis, S. N. (1998). *Atmospheric Chemistry and Physics*. John Wiley, New York.

Stelson, A. W. and Seinfeld, J. H. (1982). Thermodynamic Prediction of the Water Activity, Nh4no3 Dissociation-Constant, Density and Refractive-Index for the Nh4no3-(Nh4)2so4-H2o System at 25-Degrees-C. *Atmos. Environ.*, 16:2507–2514.

Szoke, R., Alfoldy, B., Balashazy, I., Hofmann, W., and Sziklai-Laszlo, I. (2007). Size Distribution, Pulmonary Deposition and Chemical Composition of Hungarian Biosoluble Glass Fibers. *Inhal. Toxicol.*, 19:325–332.

Venkataraman, C. and Raymond, J. (1998). Estimating the Lung Deposition of Particulate Polycyclic Aromatic Hydrocarbons Associated with Multimodal Urban Aerosols. *Inhalation Toxicol.*, 10:183–204.

Wang, C. S. (1975). Gravitational Deposition of Particles from Laminar Flows in Inclined Channels. *J. Aerosol Sci.*, 6:191–204.

Warneck, P. (1988). *Chemistry of the Natural Atmosphere*. Academic Press, San Diego, CA.

Wilson, D. W., Aung, H. H., Lame, M. W., Plummer, L., Pinkerton, K. E., Ham, W., Kleeman, M., Norris, J. W., and Tablin, F. (2010). Exposure of Mice to Concentrated Ambient Particulate Matter Results in Platelet and Systemic Cytokine Activation. *Inhal. Toxicol.*, 22:267–276.

Zhang, L. and Yu, C. P. (1993). Empirical Equations for Nasal Deposition of Inhaled Particles in Small Laboratory—Animals and Humans. *Aerosol Sci. Technol.*, 19:51–56.